Cement and Concrete Research 40 (2010) 810–819

Contents lists available at ScienceDirect

Cement and Concrete Research

journal homepage: http://ees.elsevier.com/CEMCON/default.asp

Orientation factor and number of fibers at failure plane in ring-type steel fiber reinforced concrete

C. Lee *, H. Kim

School of Architecture and Building Science, Chung-Ang University, Seoul 156-756, Republic of Korea

ARTICLE INFO

Article history:
Received 18 May 2009
Accepted 18 November 2009

Keywords:
Modeling (E)
Concrete (E)
Fiber Reinforcement (E)
Orientation Factor

ABSTRACT

Considering the probabilistic distributions of fibers in ring-type steel fiber reinforced concrete, the orientation factor and the number of ring-type steel fibers crossing the failure plane were theoretically derived as a function of fiber geometry, specimen dimensions, and fiber volume fraction. A total number of 24 specimens were tested incorporating different fiber types, specimen geometry, and fiber volume fractions of 0.2% and 0.4%: 5 beams and 5 panels containing straight steel fibers; and 6 beams and 8 panels containing ring-type steel fibers. Measurements were made to assess the number of fibers at fractured surfaces of steel fiber reinforced concrete. The developed theoretical expressions reasonably predicted the orientation factor and the number of ring-type steel fibers at failure plane: the average and the standard deviation for the ratios of the test to theory were 1.03 and 0.26, respectively. Theoretical investigations and comparisons were made for the values of orientation factor and the number of fibers at failure plane for straight steel fibers and ring-type steel fibers.

1. Introduction

Straight steel fibers (SSFs) increase tensile strength of concrete by arresting and deflecting microcracks developing in concrete under external load effects [1–4]. Their lengths are usually short to avoid inadequate workability of the concrete mixture and non-uniform fiber distribution due to fiber balling during the mixing process [5]. The post-peak behavior of straight steel fiber reinforced concrete (SSFRC) is mainly governed by tensile resistance of SSFs crossing the failure plane. In general, yielding of SSFs rarely occurs. Instead, SSFs at critical section are pulled out due to insufficient embedded length of the fibers.

Recently, ring-type steel fibers (RSFs) have been developed to overcome the limitations associated with traditional SSFs. While the mechanical performance of SSFs relies mainly on the fiber–matrix interfacial bond strength and pull-out resistance, RSFs are intended to achieve a more desirable resisting mechanism other than pull-out. According to the flexural test results by Choi and Lee [6], ring-type steel fiber reinforced concretes (RSFRCs) have shown three distinctive failure patterns: fiber rupture after yielding; cone-type concrete fracture; and separation between RSFs and surrounding concrete matrix. Failure mechanisms of RSFRC did not involve pull-out resistance as in conventional SSFRC.

Flexural toughness has been recognized as an important characteristic for which SFRCs are noted [7]. Since improvements to residual strength reflect an ability to carry more tensile loads after cracking, this results in a material which can exhibit better toughness, fatigue resistance, impact resistance, and additional load-bearing capacity which is in direct proportion to the toughness that the steel fibers impart to the concrete [8,9]. Experimental comparisons on flexural toughness have shown that RSFRCs exhibited higher toughness than SSFRCs with hooked end straight steel fibers for volume fractions of 0.2% and 0.4% [6].

It has been known that mechanical properties of SFRC are correlated with some measures representing the spacing of fibers in concrete or the number of fibers per unit area. According to the spacing concept [10], closely spaced fibers locally restrain the internal flaws and prevent them from extending into the adjacent material in the pre-peak stage. Better post-peak behavior is also anticipated with a larger number of fibers crossing the failure plane. For SSFRC, as a larger number of fibers cross the failure plane in the post-peak region, more fiber pull-out resistance would be activated, leading to an improved toughness. For RSFRC, better toughness would be expected with a larger number of RSFs at failure plane by mobilization of fiber rupture, cone-type concrete fracture, and separation between RSFs and surrounding concrete matrix.

Randomly distributed fibers in concrete matrix, however, may result in a different number of RSFs crossing the failure plane and consequently a different mechanical performance may be obtained even for the RSFRCs with identical mix design and fiber volume fraction. It is, therefore, important to evaluate the performance of RSFRCs by a rational assessment in regard to the number of fibers at failure plane. In order to quantify the nominal measure on the number

* Corresponding author. Tel.: +82 2 820 5872.
E-mail address: cdlee@cau.ac.kr (C. Lee).

0008-8846/$ – see front matter © 2009 Elsevier Ltd. All rights reserved.
doi:10.1016/j.cemconres.2009.11.009

of ring-type steel fibers at the failure plane, theoretical expressions for the orientation factor and the number of fibers at the failure plane are derived in this investigation.

2. Development of theoretical expressions

2.1. Number of fibers per unit area, aligned in the tensile direction

When RSFs are distributed uniformly at random in concrete, the centroid of each RSF will locate within the cube of l_c^3 as shown in Fig. 1. If the total number of RSFs in the specimen of $b \times h \times l$ is N_{RT}, the following expressions can be derived:

$$N_{RT} \cdot l_c^3 = b \cdot h \cdot l \tag{1a}$$

$$A_{f,R} \cdot l_{f,R} \cdot N_{RT} = V_f \cdot b \cdot h \cdot l \tag{1b}$$

where:

$A_{f,R}$ sectional area of fiber forming a RSF;
$l_{f,R}$ perimeter of a RSF $= 2\pi \cdot r_R$;
r_R radius of RSF; and
V_f volume fraction of fiber.

From Eqs. (1a) and (1b), the lateral dimension of each cube can be estimated as

$$l_c = \sqrt[3]{\frac{A_{f,R} \cdot l_{f,R}}{V_f}}. \tag{2}$$

If all RSFs are aligned in the tensile direction, the number of RSFs crossing the unit failure plane ($n_{R,A}$) can be obtained as

$$n_{R,A} = \left(\frac{b}{l_c} \cdot \frac{h}{l_c}\right) \cdot \left(\frac{2 \cdot r_R}{l_c}\right) / (b \cdot h) = \frac{2 \cdot r_R}{l_c^3}. \tag{3}$$

By substituting l_c in Eq. (2) into Eq. (3), we get

$$n_{R,A} = \frac{1}{\pi} \cdot \frac{V_f}{A_{f,R}} \tag{4}$$

The number of straight steel fibers that are aligned in the tensile direction ($n_{S,A}$) can be obtained by replacing $l_{f,R}$ in Eq. (1b) and Eq. (2) with their length, $l_{f,S}$:

$$n_{S,A} = \left(\frac{b}{l_c} \cdot \frac{h}{l_c}\right) \cdot \left(\frac{l_{f,S}}{l_c}\right) / (b \cdot h) = \frac{l_{f,S}}{l_c^3} \quad \text{or} \tag{5a}$$

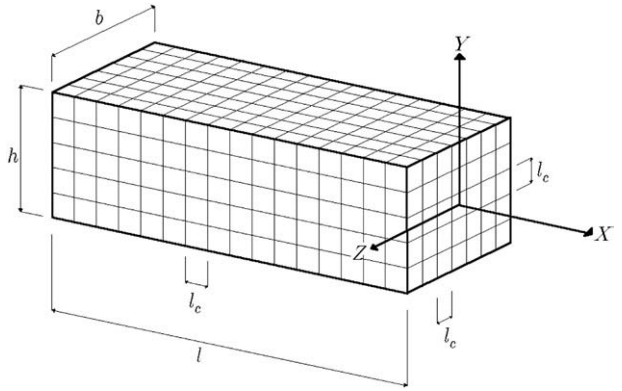

Fig. 1. Cubes of l_c^3 containing centroids of RSFs distributed uniformly at random in concrete specimen of $b \times h \times l$.

$$n_{S,A} = \frac{V_f}{A_{f,S}} \tag{5b}$$

where:

$A_{f,S}$ cross sectional area of SSF.

Comparison between Eq. (4) and Eq. (5b) reveals that if fibers are all aligned in the tensile direction, 3.14 times more SSFs than RSFs would cross the unit area of the failure plane. This is because more SSFs are available than RSFs in the specimen given for the same volume fraction and the cross sectional area of fibers.

2.2. Number of fibers per unit area, with random orientation

When fibers are randomly distributed in concrete, the number of fibers per unit cross sectional area can be modified as

$$n_S = \alpha_S \cdot \frac{V_f}{A_{f,S}} \text{ for SSF} \tag{6a}$$

$$n_R = \alpha_R \cdot \frac{1}{\pi} \cdot \frac{V_f}{A_{f,R}} \text{ for RSF} \tag{6b}$$

where:

α_S and α_R orientation factors for SSF and RSF, respectively (≤ 1.0).

The orientation factor takes into account the randomness of fibers in their orientation with respect to the tensile direction and its effect on the amount of fibers crossing the failure plane. For SSF, the orientation factor has been known to be influenced by both fiber and specimen geometries. The following orientation factor, simplified by the expansion of Taylor series for practical application, has been suggested by Soroushian and Lee [11] for the SSF in the rectangular SFRC specimen with its sectional width (b) greater than the length of straight steel fiber ($l_{f,S}$)

$$\alpha_s = \begin{cases} \frac{l_{f,S}}{h} \cdot \tan^{-1}\left(\frac{h}{\sqrt{6} \cdot l_{f,S}}\right) \cdot \left(1.56 + 0.766 \cdot \frac{l_{f,S}}{b}\right) & \text{if } h \leq l_{f,S} \\ 0.098 \cdot \frac{l_{f,S}^2}{b \cdot h} + 0.2 \cdot l_{f,S} \cdot \frac{(b+h)}{b \cdot h} + 0.405 & \text{if } h > l_{f,S} \end{cases} \tag{7}$$

where:

h depth of the specimen.

For a three dimensional (3-D) case, the rotation of a SSF in both θ_y- and θ_z-directions affects the crossing of a SSF at the failure plane (Fig. 2(a)). For a RSF, however, crossing the failure plane depends on the rotation in θ_z-direction only (Fig. 2(b)). As an extreme case, if the specimen thickness is small enough to restrict the orientation of SSFs out of the X–Z plane in which fibers are contained, all SSFs will be oriented in two dimensional (2-D) random orientations (Fig. 3(a)). In this case, the orientation factor for SSF was given as follows [11]:

$$\alpha_S = \frac{\int_0^{\pi/2} \frac{l_{f,S}}{2} \cdot \cos\theta_y \cdot d\theta_y}{\int_0^{\pi/2} \frac{l_{f,S}}{2} \cdot d\theta_y} = 0.64. \tag{8}$$

For RSFs in 2-D condition (Fig. 3(b)), the orientation of a RSF is not influenced by the fiber rotation in θ_y-direction and consequently the orientation factor remains as 1.0.

$$\alpha_R = 1.0 \tag{9}$$

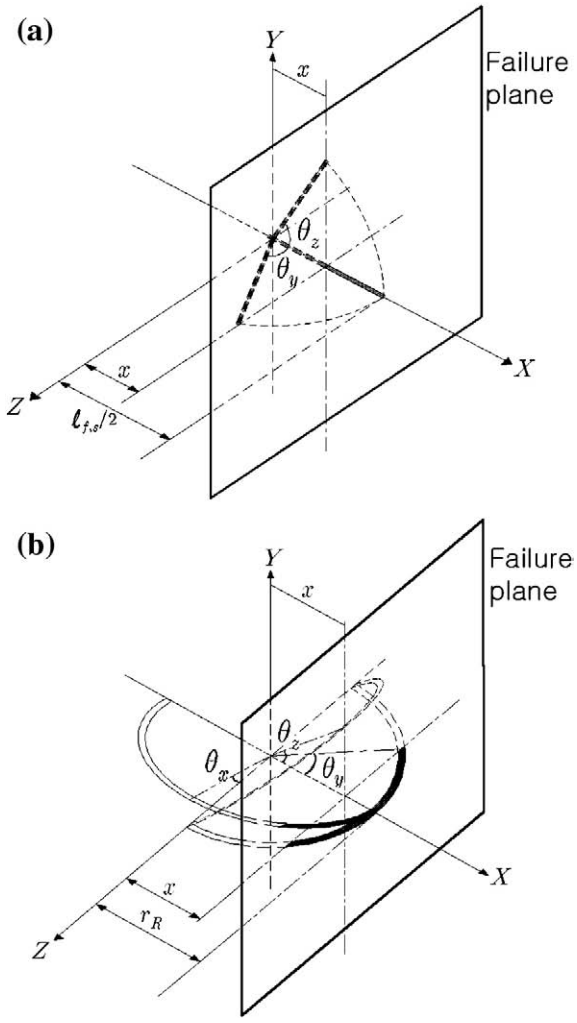

Fig. 2. Orientations of fiber and their effects on the fiber crossing at failure plane: (a) SSF; (b) RSF.

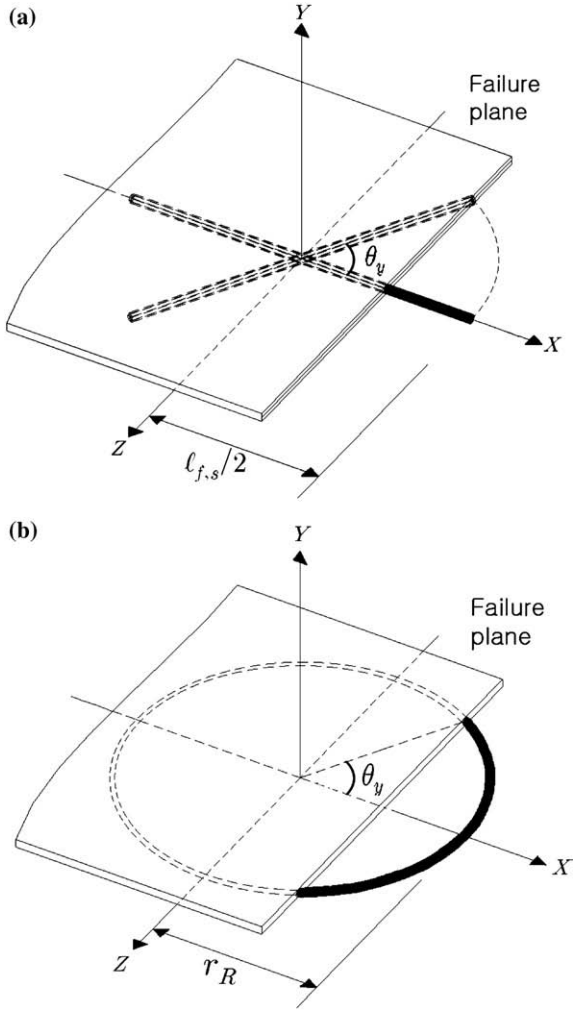

Fig. 3. Fiber orientation in 2-D condition: (a) SSF; (b) RSF.

It is interesting to observe that in the 2-D condition, the orientation factor for RSF is 1.0/0.64 = 1.56 times greater than that of SSF. Substitution of these values into Eqs. (6a) and (6b) shows that given the same volume fraction and the same sectional area of fibers, the number of SSFs crossing the unit area of the failure plane in 2-D condition is two times as many as that of RSFs.

When there are four closely spaced boundaries, there are more restrictions on random orientation of fibers, giving the values of the orientation factor between 2-D and 3-D conditions. Consequently, the number of fibers crossing the unit failure plane is influenced by the boundary conditions. In the following sections, the number of RSFs crossing the failure plane is theoretically developed based on the probability concept that considers the effect of boundaries in reorienting RSFs near the boundaries to the direction parallel to the boundaries.

2.2.1. The probability for a RSF to cross the failure plane without boundary restrictions

For a RSF whose centroid is located at a distance x ($\leq r_R$) away from the failure plane that is parallel to Y–Z plane (Fig. 4), the maximum rotation of the RSF with respect to Z-axis to cross the failure plane is

$$\theta_z = \cos^{-1}(x / r_R). \tag{10}$$

The probability of the RSF with its centroid at a distance x ($\leq r_R$) away from the failure plane and subjected to a random rotation with respect to Z-axis, is, therefore

$$p_{\vartheta_z} = \frac{\theta_z}{(\pi/2)} = \frac{2}{\pi} \cdot \cos^{-1}(x / r_R). \tag{11}$$

Since the failure plane can be anywhere between $0 \leq x \leq r_R$, the overall probability that the RSF, without any boundary restrictions on its orientation, would cross the failure plane in the matrix becomes

$$P_D = \int_0^{r_R} \frac{2}{\pi} \cdot \cos^{-1}(x / r_R) \cdot dx / \int_0^{r_R} dx = 0.64. \tag{12}$$

2.2.2. The probability for a RSF to cross the failure plane with boundary restrictions

Fig. 5(a) shows a RSF near the boundary of the specimen whose depth is greater than the diameter of RSF ($h > 2 \cdot r_R$). If the centroid of a RSF is located at a distance of r_R or farther from the boundary in Y-direction, the RSF is free in its rotation and is not subject to the boundary restrictions in its orientation. Otherwise, the rotation of the RSF is restricted by the boundary and thus those RSFs that are located closer to the boundary would have more chance to cross the failure plane. When the centroid of a RSF is located at $(X, Y, Z) = (0, y_F, 0)$ as shown in Fig. 5(a), its rotation is restricted by the boundary and the probability of crossing the failure plane is 1.0. In fact, the fibers whose

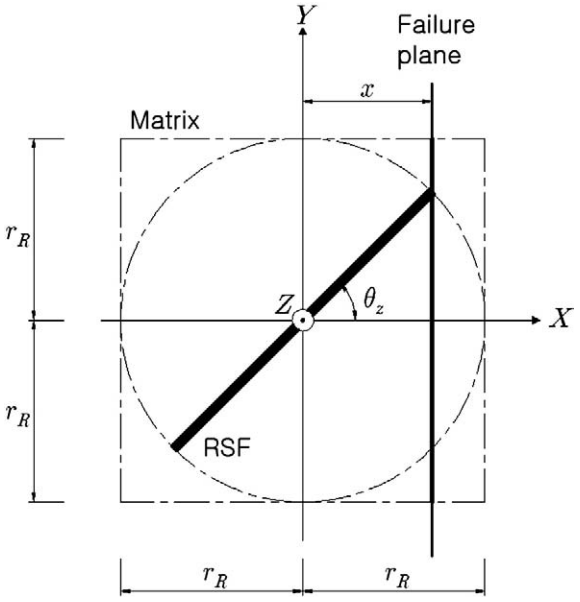

Fig. 4. Rotation of RSF about the *Z*-axis near the failure plane without boundary restriction.

centroids are located above the y_F ($y_F \le y \le r_R$) will all cross the failure plane. If the centroid of a RSF is located below the y_F, (i.e., $0 \le y < y_F$), the RSF has more freedom to rotate from the failure plane with $\theta_z > \theta_F$ (Fig. 5(a)). The RSF, thus, has a probability less than 1.0 to cross the failure plane. Such a RSF has a probability of crossing the failure plane as given below:

$$p_{\vartheta_z} = \frac{\theta_F}{\theta_z} \quad \text{for } 0 \le y < y_F \tag{13}$$

where:

θ_F $\cos^{-1}(x/r_R)$; and
θ_z $\sin^{-1}(1-y/r_R)$.

Note that P_{ϑ_z} becomes zero for $x = r_R$ and approaches to 1.0 if x gets closer to zero. For the fixed location of the failure plane at $X = x$, the probability of the RSF with its centroid at $(X, Y, Z) = (0, y, 0)$ for $0 \le y \le r_R$ can be expressed as follows.

$$p_B = \begin{cases} 1.0 & \text{if } y_F \le y \le r_R \\ \left\{ \int_0^{y_F} \frac{\cos^{-1}(x/r_R)}{\sin^{-1}(1-y/r_R)} \cdot dy + \int_{y_F}^{r_R} (1.0) \cdot dy \right\} \Big/ \int_0^{r_R} dy & \text{if } 0 < y < y_F \end{cases} \tag{14}$$

where:

y_F $r_R \cdot (1 - \sin(\cos^{-1}(x/r_R)))$

Since the failure plane can pass through anywhere between $0 \le x \le r_R$, the overall probability of the RSF to cross the failure plane becomes

$$P_B = \left\{ \int_0^{r_R} \int_{y_F}^{r_R} (1.0) \cdot dy \cdot dx + \int_0^{r_R} \int_0^{y_F} \frac{\cos^{-1}(x/r_R)}{\sin^{-1}(1-y/r_R)} \cdot dy \cdot dx \right\} \Big/ \left(\int_0^{r_R} \int_0^{r_R} dy \cdot dx \right)$$
$$= 0.93 \text{ for } b > 2 \cdot r_R \text{ and } h > 2 \cdot r_R \tag{15}$$

If the depth of the specimen is less than or equal to the diameter of RSF ($h \le 2 \cdot r_R$), more fibers would be restricted to the direction parallel to the boundary as shown in Fig. 5(b). The overall probability of a RSF to cross the failure plane for $h \le 2 \cdot r_R$ can be obtained as Eq. (16) by taking the similar approach for the case with $h > 2 \cdot r_R$.

$$P_B = \left\{ \int_0^{x_L} \int_0^{h/2} (1.0) \cdot dy \cdot dx + \int_{x_L}^{r_R} \left[\int_0^{y_F} \frac{\cos^{-1}(x/r_R)}{\sin^{-1}((h/2-y)/r_R)} \cdot dy + \int_{y_F}^{h/2} (1.0) \cdot dy \right] \cdot dx \right\}$$
$$\div \int_0^{r_R} \int_0^{h/2} dy \cdot dx \quad \text{for } b > 2 \cdot r_R \text{ and } h \le 2 \cdot r_R \tag{16}$$

where:

x_L $r_R \cdot \cos(\sin^{-1}(h/(2 \cdot r_R)))$.

2.2.3. The number of RSFs crossing the failure plane and the orientation factor

Fig. 6 represents a failure plane of a rectangular specimen with b and $h > 2 \cdot r_R$, whose failure plane is divided with different regions: regions with and without boundary restrictions. While the orientation of RSFs, with their centroids being located within the radius of RSF from the boundary, is restricted by the boundary, the rest of the RSFs with their centroids away from these regions are free in their orientation. The expected total number of RSFs crossing the failure plane (N_R) can be obtained by summing the products of the appropriate probability of a RSF to cross the failure plane and the number of RSFs in the corresponding region. Referring to Fig. 6 and using Eqs. (12) and (15), the expected number of RSFs at the failure plane can be found for the specimen with b and $h > 2 \cdot r_R$ as

$$N_R = \frac{2 \cdot r_R}{l_c} \times \left\{ P_D \cdot \frac{(b-2 \cdot r_R) \cdot (h-2 \cdot r_R)}{l_c^2} + P_B \cdot \left(2 \cdot \frac{b \cdot r_R}{l_c^2} + 2 \cdot \frac{h \cdot r_R}{l_c^2} - 4 \cdot \frac{r_R^2}{l_c^2} \right) \right\}$$
$$= \frac{1}{\pi} \cdot \frac{V_f}{A_{f,R}} \cdot (0.64 \cdot b \cdot h + 0.58 \cdot r_R \cdot (b + h) - 1.16 \cdot r_R^2) \tag{17}$$

The number of RSFs crossing the unit area of the failure plane (n_R) can be obtained by dividing N_R in Eq. (17) by the sectional area of the specimen.

$$n_R = \frac{1}{\pi} \cdot \frac{V_f}{A_{f,R}} \cdot \left\{ 0.64 + 0.58 \cdot \frac{r_R \cdot (b + h)}{b \cdot h} - 1.16 \cdot \frac{r_R^2}{b \cdot h} \right\} \tag{18}$$

From Eqs. (18) and (6b), the orientation factor for the RSF can be evaluated as

$$\alpha_R = \pi \cdot \frac{A_{f,R}}{V_f} \cdot n_R$$
$$= 0.64 + 0.58 \cdot \frac{r_R \cdot (b + h)}{b \cdot h} - 1.16 \cdot \frac{r_R^2}{b \cdot h} \cdot \tag{19}$$

It is worth mentioning that while the number of RSFs crossing the failure plane is a function of specimen dimensions, radius of RSF, sectional area of fiber, and volume fraction of RSFs, their orientation factor is a function of radius of RSF and sectional dimensions of the specimen only.

If the sectional dimensions of a specimen become relatively large compared to the radius of RSF and fibers are in the condition of free rotation with minimal boundary restrictions (3-D condition approximately), α_R approaches to 0.64 corresponding to the value of the orientation factor for SSF in the 2-D condition. In such a case, the orientation of RSF is approximately 1.57 (=0.64/0.405) times more effective than that of SSF.

For the rectangular specimen with $b > 2 \cdot r_R$ and $h \le 2 \cdot r_R$, the numerical integration scheme was employed to find the values of Eq. (16) for different ratios of h/r_R at an interval of 0.1. The results

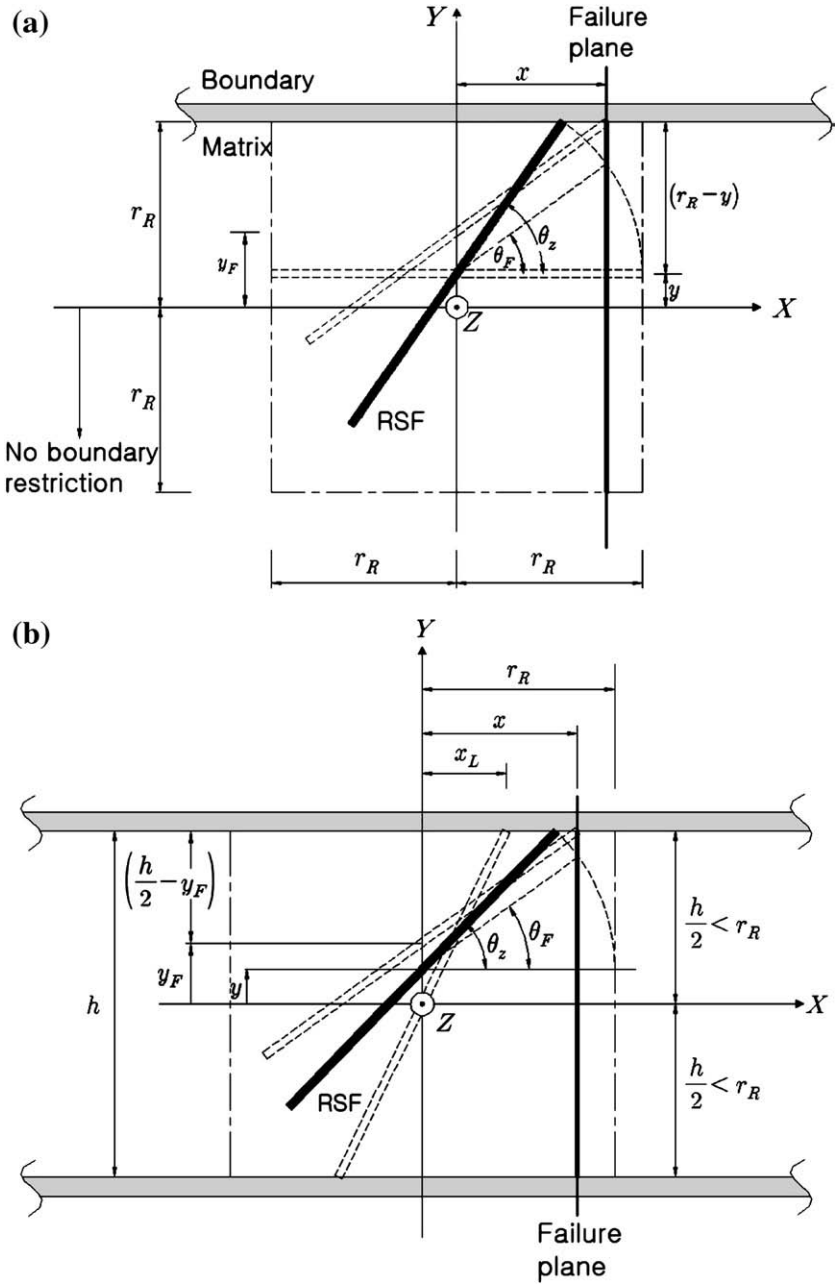

Fig. 5. Rotation of RSF about the *Z*-axis near the failure plane with boundary restriction: (a) $h>2\cdot r_R$; (b) $h\leq 2\cdot r_R$.

were then interpolated with a quadratic function of h/r_R as given in Eq. (20) for practical use.

$$P_B = -0.022\cdot(h/r_R)^2 + 0.011\cdot(h/r_R) + 1.0 \quad (20)$$

Fig. 7 shows Eq. (20) interpolating numerically integrated values of Eq. (16). Note that P_B in Eq. (20) becomes 0.93 at its limiting value of $h/r_R=2.0$, which corresponds to the value given by Eq. (15). It approaches to 1.0 when h/r_R reduces to a value close to zero and this coincides with the one in the 2-D condition (see Eq. (9)). Based on Eq. (20), the total number of fibers at the failure plane, the total number of fibers at unit failure plane and the orientation factor can be obtained as follows for the rectangular specimen with $b>2\cdot r_R$ and $h\leq 2\cdot r_R$.

$$N_R = \frac{1}{\pi}\cdot\frac{V_f}{A_{f,R}}\cdot(-0.022\cdot(h/r_R)^2 + 0.011\cdot(h/r_R)+1.0)\times b\cdot h \quad (21)$$

$$n_R = \frac{1}{\pi}\cdot\frac{V_f}{A_{f,R}}\cdot(-0.022\cdot(h/r_R)^2 + 0.011\cdot(h/r_R) + 1.0) \quad (22)$$

$$\alpha_R = -0.022\cdot(h/r_R)^2 + 0.011\cdot(h/r_R) + 1.0 \quad (23)$$

3. Comparison with test results

3.1. Test specimens

In the previous research by Choi and Lee [6], comparative flexural tests were performed for different RSFRCs containing different RSFs of ring diameters (20, 30, 40, 50, and 60 mm) and fiber diameters (0.4, 0.5, 0.8 and 1.2 mm). According to their test results, optimum ring diameter appeared to be 30 mm or 40 mm for the mix. Based on their test results, dimensions of each steel fiber were determined in this

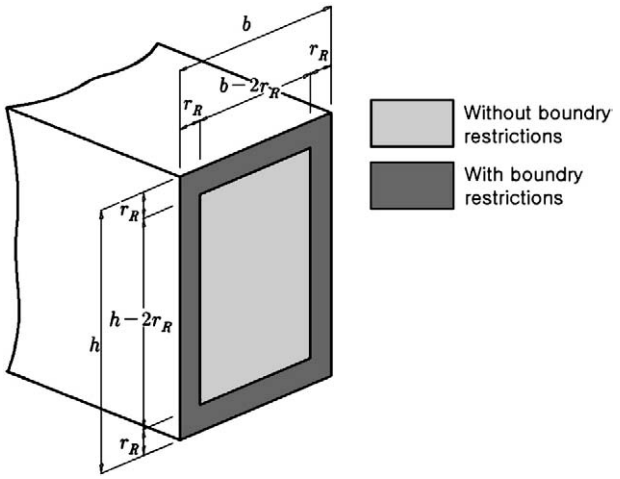

Fig. 6. Failure plane of rectangular specimen divided into regions with or without boundary restrictions ($b>2\cdot r_R$ and $h>2\cdot r_R$).

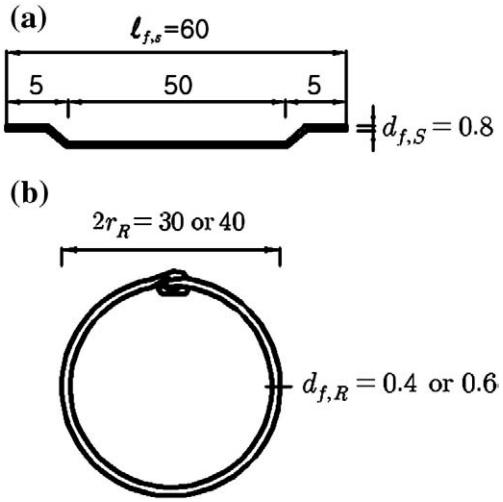

Fig. 8. Fiber configurations: (a) SSF; (b) RSF.

research. The ring diameters of 30 mm or 40 mm and the fiber diameters of 0.4 mm or 0.6 mm were used in producing RSFs. The average tensile strength of the cold-drawn wire used for RSFs was 4120 MPa. RSFs were produced by a manufacturing machine. For straight steel fibers, commercially available hooked-end straight steel fibers with 0.8 mm diameter and 60 mm length were used. Fig. 8 illustrates the configurations of different fibers tested in this research. Two different fiber volume fractions of 0.2% (15 kg/m^3) and 0.4% (30 kg/m^3) were considered for each fiber reinforced concrete.

Specimens were labeled as $S\cdot FT\cdot C\cdot D\cdot LD\cdot R$ where S stands for specimen type (B: beam type; P: panel type), FT for fiber type (H: hooked end straight steel fiber; and R: ring-type steel fiber), C for fiber contents (15: 15 kg/m^3; 30: 30 kg/m^3), D for fiber diameter (4: 0.4 mm; 6: 0.6 mm; 8: 0.8 mm), LD for either fiber length of hooked-end steel fiber (60: 60 mm in length) or diameter of ring-type steel fiber (30: 30 mm; 40: 40 mm in diameter), and R for replication (A, B or C). A total number of 24 specimens (5 beams and 5 panels for SSFRC and 6 beams and 8 panels for RSFRC) were tested. Each beam measured 550 mm long, 150 mm wide, and 150 mm deep. Dimensions of panel specimens were 300 mm long, 300 mm wide, and 50 mm deep. In Table 1, names and sectional dimensions of the test specimens are summarized. Concrete mix was designed to achieve 35.0 MPa compressive strength at 28 days. Ordinary Portland cement, river sand, and a crushed limestone coarse aggregate with 18 mm maximum grain size were used. Cement, fine aggregate, and coarse aggregate were mixed in the proportion of 1:1.92:2.36 by weight. The water-to-cement ratio was kept constant at 0.48.

The content of fibers in the mix was measured in their mass per unit volume. The preparation of all the mixes was essentially similar. Firstly, the abovementioned mix was prepared, then the fibers were uniformly fed into the mix by hand. Minor balling was observed during mixing although good workability of SFRC without dosing any superplasticizer would have been expected. Test specimens were compacted on a vibrating table. All specimens were moisture-cured for 72 h and then demolded. After 28 days of air curing in the laboratory environment at 23±2 °C, all specimens were tested in flexure within 35 days of age.

Each beam specimen was tested under four-point loading and each panel specimen under three-point loading. The testing system was a computer-controlled closed-loop servo-hydraulic universal testing machine. The test arrangements are shown in Fig. 9. The tests were continued until the complete fracture occurred by the major flexural crack (Fig. 10).

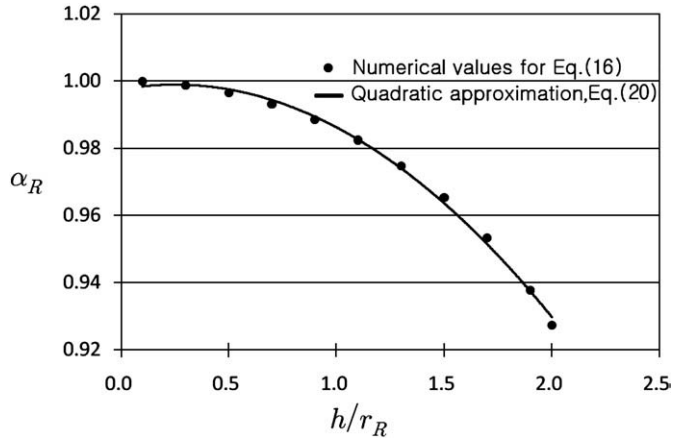

Fig. 7. Quadratic approximation of the orientation factor of RSF for $b>2\cdot r_R$ and h/r_R less than 2.0.

3.2. Number of fibers at failure plane and orientation factor

In Table 1, experimentally measured and theoretically assessed numbers of fibers and orientation factors at the failure plane are tabulated along with those parameters required for the theoretical assessment. Note that ratios of tested to theoretical values in Table 1 correspond to both the number of fibers at the failure plane and the orientation factor (see Eqs. (17) and (19) for RSF). The overall average value and standard deviation of the ratio of experimentally observed number (or orientation factor) of SSFs to the theoretically assessed one were 1.0 and 0.31 and those for RSFs were 1.03 and 0.26, respectively. Although the orientation factor cannot theoretically exceed 1.0, some measured values of the orientation factor were greater than 1.0 in those specimens of PH15860C, PR15640A, PR15640B, and PR30640A. Although overall averages were close to 1.0 for the ratios of experimentally observed and theoretically assessed number of fibers (or orientation factors) at the failure plane, their distributions were characterized with large standard deviations of 0.31 for SSFs and 0.26 for RSFs, respectively. This might be due to the random nature of fiber distributions, which sometimes leads fibers to concentrate at a certain region in concrete matrix and, thus, to disturb the uniformity of the number of fibers crossing the failure plane. This also implies that mechanical properties of SFRC, which have been reported to have some correlations with the number of fibers at the failure plane [11], need to be calibrated on the basis of theoretical measure which can take into account the statistical

Table 1
Specimen names and test results.

Specimen names	Specimen dimensions (mm)	Number of fibers/specimens	Parameters			Number of fibers at failure plane		Orientation factors		Test
	$b\times h\times l$	N_f	$l_{f,s}$ or $2r_R$	$l_{f,s}/b$ or r_R/b	$l_{f,s}/h$ or r_R/h	Tests	Theory	Tests	Theory	Test/Theory
BH15860A	150×150×550	820	60.0	0.4	0.4	47	52.0	0.52	0.58	0.90
BH15860B						49		0.55		0.95
BH15860C						68		0.76		1.31
Average						55		0.61		1.05
BH30860A		1,640	60.0	0.4	0.4	105	104.0	0.59	0.58	1.02
BH30860B						76		0.42		0.72
Average						91		0.51		0.87
PH15860A	300×50×300	298	60.0	0.2	1.2	38	40.2	0.64	0.67	0.96
PH15860B						42		0.70		1.04
PH15860C						68		1.14		1.70
Average						49		0.83		1.23
PH30860A		596	60.0	0.2	1.2	60	80.5	0.50	0.67	0.75
PH30860B						51		0.43		0.64
Average						56		0.47		0.69
SSFRC Total average										1.00
SSFRC Standard deviation										0.31
BR15430A	150×150×550	1,987	30.0	0.1	0.1	101	84.9	0.88	0.74	1.19
BR15430B						110		0.96		1.30
BR15430C						52		0.46		0.62
Average						88		0.77		1.04
BR30430A		3,974	30.0	0.1	0.1	151	169.9	0.66	0.74	0.89
BR30430B						125		0.55		0.74
BR30430C						114		0.50		0.68
Average						130		0.57		0.77
PR15430A	300×50×300	723	30.0	0.05	0.3	56	62.7	0.74	0.83	0.89
PR15430B						65		0.86		1.04
Average						61		0.80		0.96
PR15640A		241	40.0	0.07	0.4	35	29.7	1.04	0.88	1.18
PR15640B						43		1.28		1.45
Average						39		1.16		1.32
PR30430A		1,447	30.0	0.05	0.3	112	125.5	0.74	0.83	0.89
PR30430B						128		0.85		1.02
Average						120		0.80		0.96
PR30640A		482	40.0	0.07	0.4	74	59.4	1.24	0.88	1.41
PR30640B						66		0.98		1.11
Average						70		1.11		1.26
RSFRC Total average										1.03
RSFRC Standard deviation										0.26

properties on the distribution of fibers in matrix. In Fig. 11, comparisons were made for the load–deflection curves of the tested SFRCs having the identical volume fractions but with a different number of fibers measured at the failure plane. The numbers in parentheses in Fig. 11 represent the total number of fibers experimentally observed at both sides of the failure plane of the specimens. It can be seen that the specimens with more fibers at the failure plane maintained higher toughness in the post-peak region. The theoretical expressions developed in this study can provide the nominal measure on the number of fibers at the failure plane and can be used as an estimator for justifying the experimentally obtained mechanical properties of RSFRC in relation to the measured number of fibers at the failure plane.

4. Theoretical investigation of the orientation factors and the number of fibers for unit area of the failure plane

Investigations and comparisons are made for the orientation factor and the number of fibers for RSF and SSF based on the theoretical expressions presented in this research.

4.1. Size effect on the orientation of RSF

Fig. 12 illustrates the changes in the values of orientation factor for RSF (α_R) as the specimen dimensions relative to the radius of RSF vary in $2.0 \le b/r_R \le 50$ and $0.1 \le h/r_R \le 50$. When the ratio h/r_R approaches close to zero (i.e., the 2-D condition), the value of orientation factor becomes close to 1.0 for all b/r_R values. When both width and depth of the specimen become relatively large, the orientation factor approaches to an asymptotic value of 0.64, which corresponds to the value of the orientation factor for the 3-D condition without boundary restrictions.

In Fig. 13(a), the values of the orientation factor were plotted for typical test beam specimens ($\alpha_{R,T}$) used in flexural tests (width (b) × depth (h) = 100 mm × 100 mm or 150 mm × 150 mm) and for the structural member ($\alpha_{R,S}$) whose width (B) is arbitrarily fixed at 1000 mm but its depth (H in mm) is allowed to vary from 100 mm to 1000 mm for illustrative purpose. Two different radii of RSF were considered: $r_R = 15$ mm and 30 mm. According to Fig. 13(a), those structural members with a relatively smaller depth (H) than the depth of the test beam specimens would have larger values of the orientation factor than the test beam specimens. On the other hand, when the structural depth greatly increases compared to the depth of the test beam specimens, the values of the orientation factor in the structural member tend to deviate from those of test specimens to smaller values. Fig. 13(b) compares the ratios of the orientation factor of a structural member to those of a test beam specimen considered in Fig. 13(a). Depending on the structural depth and fiber ring diameter, the ratio ranges from between 1.13 and 1.35 for shallow structural member depth to between 0.76 and 0.89 for large depth. This tendency might be referred to as 'size effect' since different fiber orientations or the degree of fiber alignment in structural members than that in test beam specimens would lead to different mechanical properties even for the same mix condition and the fiber volume fraction. Due consideration, therefore, must be given for interpreting

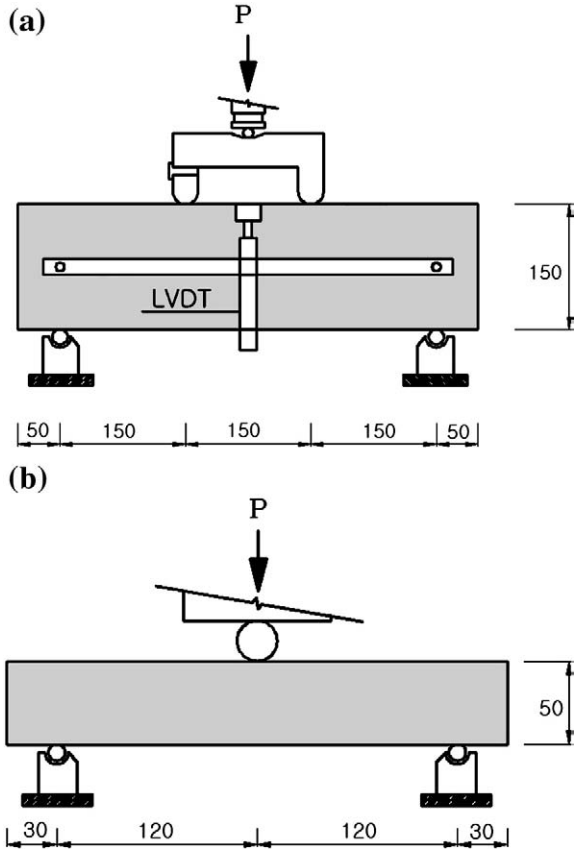

Fig. 9. Flexural test arrangements: (a) beam type specimen; (b) panel type specimen.

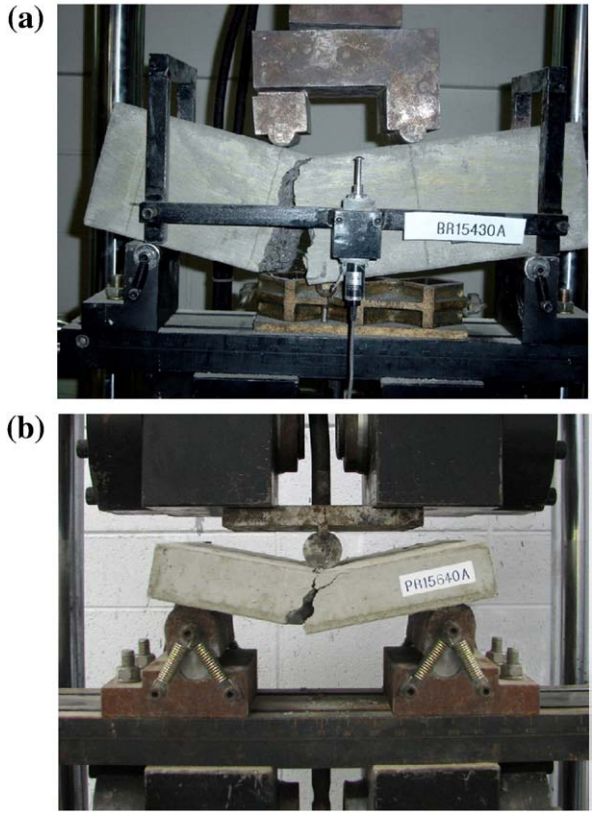

Fig. 10. Fractured specimens after test: (a) beam type specimen; (b) panel type specimen.

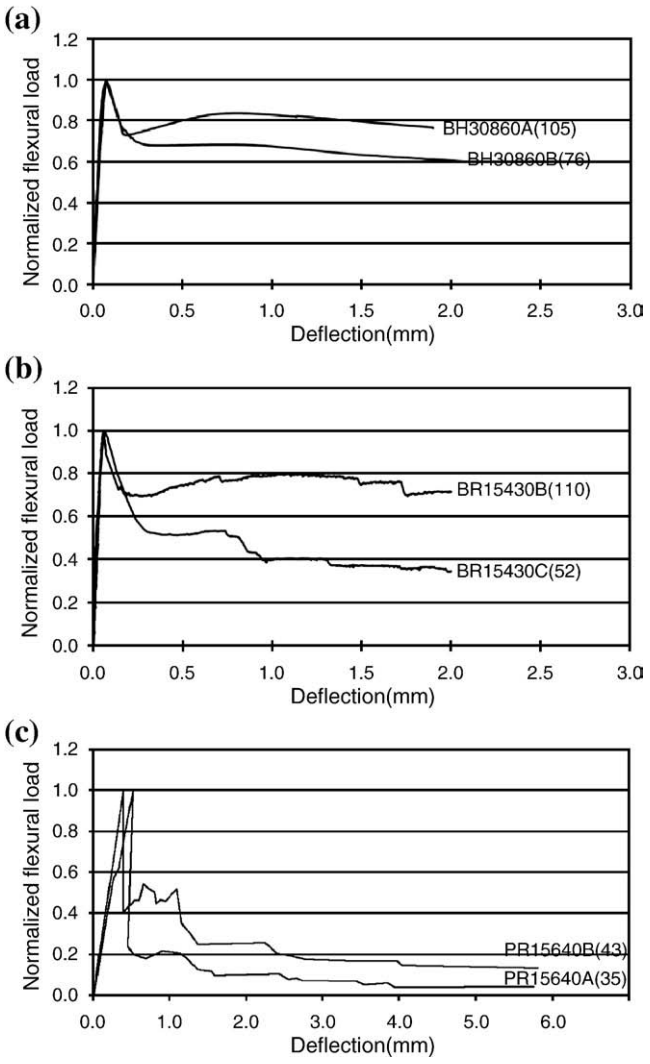

Fig. 11. Load–deflection curves: (a) BH30860; (b) BR15430; (c) BR15640.

the mechanical property of a test specimen in relation to that of RSFRCs used for a structural member whose sectional dimensions are significantly different enough to alter the levels of fiber alignment encountered in the test beam specimen. Favorable mechanical properties obtained from the test specimens, in which more fibers tend to reorient to the tensile stress direction by the boundary

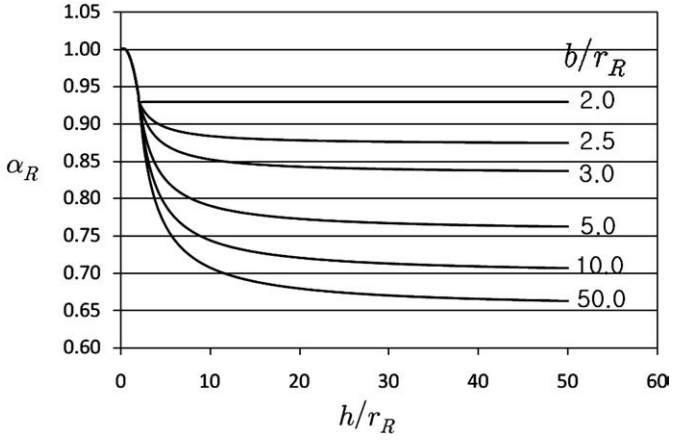

Fig. 12. Values of orientation factor of RSF (α_R) for b/r_R and h/r_R between 2.0 and 50.

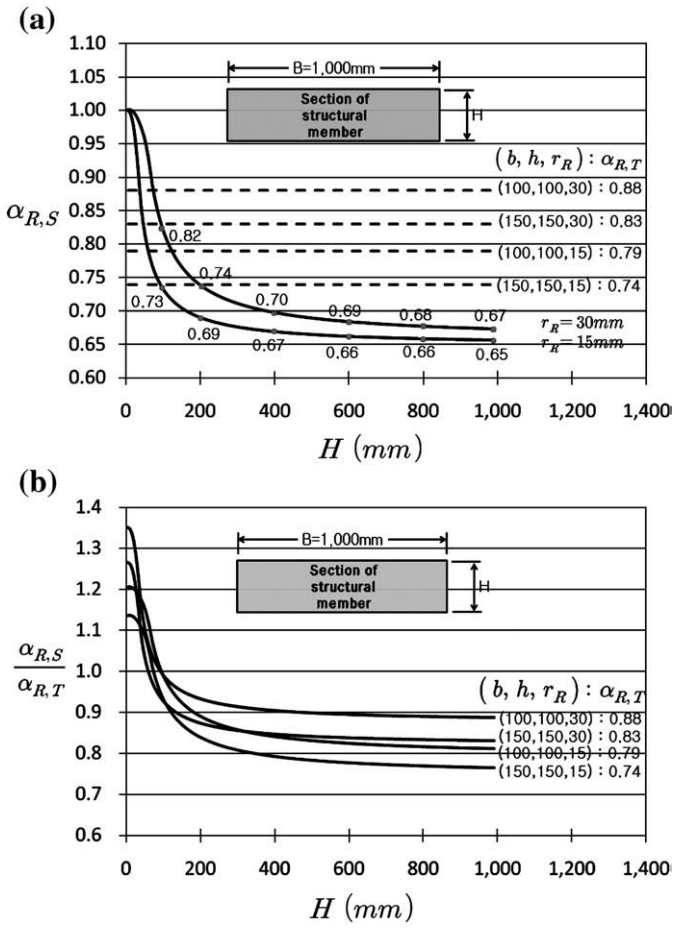

Fig. 13. "Size effect" on orientation factor: (a) orientation factors of test beam specimen ($\alpha_{R,T}$)and structural member ($\alpha_{R,S}$); (b) ratios of orientation factor for test beam specimen to that for structural member ($\alpha_{R,T}/\alpha_{R,S}$).

restrictions, would lead to an un-conservative design of structural members with larger sectional dimensions and vice versa.

4.2. Comparisons between SSF and RSF

Fig. 14 shows the changes in the ratio of the orientation factor for RSF to that for SSF (α_R/α_S). Two different radii of RSF (r_R = 15 mm and 30 mm) and two different fiber lengths of SSF ($l_{f,S}$ = 30 mm and 60 mm) were considered. It can be seen in Fig. 14 that the orientation factor of RSF possesses higher values than that of SSF for those fibers considered in this study. The ratio of the orientation factor of RSF to SSF (α_R/α_S) ranges between 1.53 and 1.62 at large structural depth H, with a higher value for a higher ratio of $r_R/l_{f,S}$. Their limiting values at large structural depth seem to approach 1.58 (=0.64/0.405) which is the ratio of orientation factor of RSF to that of SSF in 3-D condition. The ratios of the number of RSF to that of SSF at the unit area of the failure plane (n_R/n_S) are plotted in Fig. 15 for the same sectional dimensions and fibers considered in Fig. 14. For the changes of the structural depth, similar trends are observed for n_R/n_S as that of α_R/α_S. Although RSFs are more favorably oriented with respect to tensile stress direction than SSFs, most n_R/n_S values remain between 0.4 and 0.58 for relatively smaller structural depths and approach a value close to 0.5 as the structural depths increase. This is attributed to the smaller number of RSFs than SSFs in the matrix as noted in Eqs. (6a) and (6b). Fig. 15 shows that the disadvantage of using RSF with a relatively smaller radius than the longer SSF, in terms of the number of fibers at the failure plane, can be alleviated as the depth of the structural member becomes larger. It is worth mentioning, however,

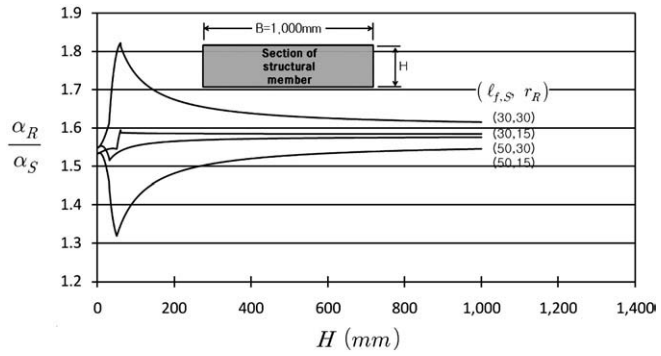

Fig. 14. Changes in the ratio of the orientation factor for RSF to that for SSF (α_R/α_S).

that RSF exhibits different resisting mechanisms than SSF which mainly relies on pull-out resistance in the post-peak loading stage. Tensile resisting mechanisms of RSF, based on fiber rupture after yielding, cone-type concrete fracture, and separation between RSF and surrounding concrete matrix, have been experimentally shown to lead RSFRC to a composite material with higher flexural toughness than SSFRC in an equivalent condition [6]. This seems to compensate for the smaller number of RSFs than SSFs at the failure plane. The interactions between the number of RSFs and different resisting mechanisms of RSF at the failure plane need to be further investigated in future studies.

5. Conclusions

The following conclusions were made from this study.

1. The orientation factor and the number of RSFs crossing the failure plane were theoretically derived as a function of fiber geometry, specimen dimensions, and fiber volume fraction. The developed theoretical expressions reasonably predicted the orientation factor and the number of RSFs at the failure plane: the average and standard deviation for the ratio of the theory to the experiments were 1.03 and 0.26, respectively, for both the orientation factor and the number of fibers at the failure plane.
2. In 2-D condition, the orientation factor of RSF is 1.0 and 1.56 times greater than 0.64 of SSF.
3. In 3-D condition, the orientation factor of RSF approaches 0.64 corresponding to the orientation factor of SSF in 2-D condition. In 3-D condition, the orientation of RSF is 1.57 times more effective than that of SSF. The orientation of RSF in 3-D condition maintains its superiority over that of SSF at the same level as in 2-D condition.
4. The orientation factor of RSF was found to possess a higher value than that of SSF for those fibers considered in this study. The ratio of the orientation factor of RSF to SSF (α_R/α_S) ranges between 1.53 and 1.62 at large structural depth, with higher value for higher

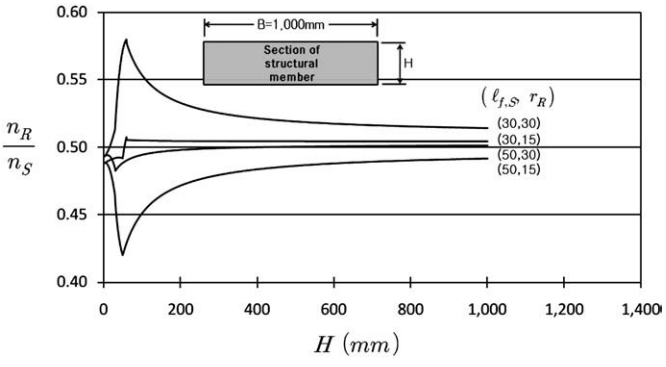

Fig. 15. The ratios of the number of RSF to that of SSF at unit failure plane (n_R/n_S).

ratio of $r_R/l_{f,S}$. Their limiting values at large depth approached 1.58 which is the ratio of orientation factor of RSF to that of SSF in 3-D condition.

5. The number of RSFs at the failure plane in RSFRC is related to their orientation influenced by different levels of boundary restrictions for different sectional dimensions. Favorable mechanical property obtained from relatively small test beam specimens may be an overestimate of RSFRC used in structural member having large sectional dimensions. Due consideration must be given for this 'size effect' in interpreting the mechanical properties of test specimen in relation to that of RSFRCs used for structural member.
6. Although a more favorable orientation factor was observed for RSFs than SSFs, most n_R/n_S values remained between 0.4 and 0.58 for relatively smaller structural depths and approached a value close to 0.5 as the structural depths increased.
7. An unfavorable number of RSFs at the failure plane in RSFRC as compared to SSFRC seemed to be overcome by distinctive tensile resisting mechanisms of RSFs. In the previous study, it has been experimentally shown that RSFRC involves fiber rupture after yielding, cone-type concrete fracture, and separation between RSF and surrounding concrete matrix, which lead RSFRC to a composite material with higher flexural toughness than SSFRC. Further study is needed for the interactions between the number of RSFs at unit failure plane and different resisting mechanisms of RSF.
8. The theoretical expressions developed in this study can provide the nominal measure of the number of fibers at the failure plane and can be used as the estimators for justifying the experimentally obtained mechanical properties of RSFRC in relation to the observed number of fibers at the failure plane.

Acknowledgments

This research was supported by the Chung-Ang University Research Scholarship Grants in 2009.

References

[1] V.S. Gopalaratnam, S.P. Shah, Failure mechanisms and fracture of fiber reinforced concrete, Proceedings of Fiber Reinforced Concrete Symposium, November, Am. Conc. Inst. Baltimore MD, 1986, pp. 1–26.
[2] A.E. Naaman, S.P. Shah, Pull-out mechanism in steel fiber reinforced concrete, J Div ASCE 102 (8) (1976) 1537–1549.
[3] R. Narayanan, A.S. Kareen, Factors influencing the strength of steel fibre reinforced concrete, Development in Fibre Reinforced Cement and Concrete, RILEM Symposium, vol. 1 (3), 1985, pp. 1–8.
[4] P. Soroushian, Z. Bayasi, Fiber-type on the performance of steel fiber reinforced concrete, ACI Mater J 88 (2) (1991) 129–134.
[5] D.R. Lankard, Prediction of the flexural strength properties of steel fibrous concrete, Proceedings, CERL Conference on Fibrous Concrete, Construction Engineering Research Laboratory, Champaign, 1972, pp. 101–123.
[6] O.C. Choi, C. Lee, Flexural performance of ring-type steel fiber-reinforced concrete, Cem Concr Res 33 (2003) 841–849.
[7] Design considerations for steel fiber reinforced concrete, Reported by ACI Committee 544, ACI 544.4R-88, 1999.
[8] P.H. Bischoff, A.J. Valsangkar, J.A. Irring, Experimental study of concrete floor slabs on grade, 1st Structural Specialty Conference, Edmonton, Alberta, Canada, 1996, pp. 273–282.
[9] P.C. Tatnall, L. Kuitenbrouwer, Steel fiber reinforced concrete in industrial floors, Concr Int (1992) 43–47.
[10] J.P. Roumaldi, J.A. Mandel, Tensile strength of concrete affected by uniformly distributed and closely spaced short length of wire reinforcement, Am Concr Inst J Proc 61 (6) (1964) 657–671.
[11] P. Soroushian, C. Lee, Distribution and orientation of fibers in steel fiber reinforced concrete, ACI Mater J 87 (5) (1990) 433–439.